Rare Metal Materials and Engineering
Volume 55, Issue 2, February 2026
Available online at www.rmme.ac.cn

Science Press

Cite this article as: Xue Lipan, Zhang Fengying, Deng Yulin, et al. Effect of Cyclic Heat Treatment on Fatigue Crack Growth Rate of Ti-6Al-4V-1Mo Alloy Prepared by Laser Directed Energy Deposition[J]. Rare Metal Materials and Engineering, 2026, 55(02): 292-301. DOI: https://doi.org/10.12442/j.issn.1002-185X.20250307.

ARTICLE

Effect of Cyclic Heat Treatment on Fatigue Crack Growth Rate of Ti-6Al-4V-1Mo Alloy Prepared by Laser Directed Energy Deposition

Xue Lipan, Zhang Fengying, Deng Yulin, Ye Zimeng, Zhao Kexin, Yu Zerong, Wu Wenlu, Su Wei, Yang Renjie

School of Materials Science and Engineering, Chang'an University, Xi'an 710064, China

Abstract: The fatigue crack growth rate of a novel Ti-6Al-4V-1Mo titanium alloy, which is developed for laser directed energy deposition technique, was investigated before and after cyclic heat treatment (CHT). Changes in microstructure, fracture surfaces, and crack growth paths were analyzed before and after CHT. Results indicate that in the stable crack growth region, the growth rates for the as-deposited and cyclic heat-treated specimens follow the relationships $da/dN=1.8651\times10^{-8}(\Delta K)^{3.2271}$ and $da/dN=1.4112\times10^{-8}(\Delta K)^{3.1125}$, respectively. Compared with that at the as-deposited state, the microstructure after CHT is transformed from a uniform basket-weave microstructure to a dual-phase microstructure consisting of near-spherical α and β-transformed matrix phases. The cyclic process also disrupts the continuity of the grain boundary α (α_{GB}) at the primary β-phase grain boundary. The coarsening of primary α and the disruption of α_{GB} continuity are the primary factors to release stress concentration and promote crack deflection, thereby decreasing the fatigue crack growth rate. Additionally, the increased occurrence of crack branching, secondary cracking, and crack bridging in cyclic heat-treated specimens further reduces the crack driving force and slows the fatigue crack growth rate.

Key words: Ti-6Al-4V-1Mo alloy; CHT; fatigue crack growth rate; laser directed energy deposition

1 Introduction

Directed energy deposition (DED), a high-energy beam-based additive manufacturing (AM) technique, has become a key method to fabricate high-performance titanium alloy components in the aerospace field due to its mold-free, near-net-shape capabilities for complex geometries[1–2]. However, the non-equilibrium solidification inherent to laser-based AM process often leads to microstructural issues in titanium alloys, especially the widely studied Ti-6Al-4V alloy, including coarse columnar grains, acicular α' martensite, and high residual stresses[3–4]. These features result in increased strength, reduced ductility, and pronounced mechanical anisotropy[5–8], thereby restricting the mechanical and fatigue performance of laser-deposited Ti-6Al-4V alloy for the aerospace applications.

Composition optimization of Ti-6Al-4V alloy for microstructure refinement and mechanical enhancement has become a significant research focus in recent years. Incorporating β-stabilizers, such as Cu[9–10], Fe[11], and Mo[12], has proven to be an effective approach to enhance the properties of AM-fabricated Ti-6Al-4V alloys. Among them, Mo can significantly refine the α-lath structure and regulate the α phase volume fraction[12–13]. In Ref. [14], the effects of Mo addition on microstructure and mechanical performance of DED-prepared Ti-6Al-4V alloy were investigated. The addition of 1wt% Mo enhanced the mechanical performance of the alloy, which yielded an ultimate tensile strength of approximately 1039 MPa and an elongation of around 13%, achieving simultaneous improvement in both strength and ductility. During the fabrication under high linear energy density condition, the Ti-6Al-4V-1Mo alloy shows a microstructure characterized by coarse α phases along grain boundaries (α_{GB}), pronounced α clusters,

Received date: May 30, 2025
Foundation item: National Key Research and Development Program of China (2024YFB4610803)
Corresponding author: Zhang Fengying, Ph. D., Professor, School of Materials Science and Engineering, Chang'an University, Xi'an 710064, P. R. China, E-mail: zhangfengying@chd.edu.cn

and thickened α laths. This structural configuration contributes to superior fracture toughness while preserving a desirable combination of strength and ductility[15].

With the development of damage-tolerance design concepts in the aerospace sector, traditional approaches focusing solely on the strength-ductility balance are no longer sufficient. Resistance against fatigue crack propagation must also be taken into consideration. Fatigue crack growth rate (FCGR) is a key indicator of damage-tolerance performance in the design methodologies. The behavior of fatigue crack growth is typically governed by both internal and external factors. Regardless of internal factor (plastic zone at the crack tip) or external factor (crack deflection), both of them are strongly influenced by the microstructure features of materials[16]. It is reported that controlling the microstructure through heat treatment (coarsening of α-laths; optimizing α distribution at grain boundaries) can effectively enhance the materials resistance against fatigue crack growth. For instance, Kim et al[17] found that annealing treatment to coarsen the α-laths in laser-deposited Ti-6Al-4V alloy effectively alleviated the crack tip stress concentration, significantly reducing FCGR. Similarly, Liu et al[18] demonstrated that the water quenching process after heat treatment at 950 °C for 1 h resulted in low aspect ratio of α-laths and discontinuous α grain boundary, which suppressed rapid fatigue crack propagation. These findings suggest that optimizing the microstructure of additively manufactured titanium alloys through heat treatment to improve fatigue crack growth resistance is a feasible approach. They also indicate that the α-laths with low aspect ratio and discontinuous coarse α grain boundary are beneficial to the enhancement in fatigue crack growth resistance of the material[19,21]. Additionally, cyclic heat treatments (CHTs) have recently been demonstrated to offer more effective microstructure control in AM $\alpha+\beta$ Ti alloys than isothermal heat treatments[20]. It is suggested that multi-step heat treatments with varying temperatures can achieve a dual-phase microstructure with different proportions of spherical α in alloys, simultaneously achieving both lath spheroidization and alloy strengthening, which can improve the fatigue performance while maintaining the high strength[22–23].

In this research, Ti-6Al-4V-1Mo alloy was fabricated via DED to investigate the appropriate CHT to produce a dual-phase microstructure consisting of near-spherical α and β-transformed matrix (β_t). The effects of CHT on the alloy microstructure and fatigue crack growth behavior were investigated. Through fracture surface analysis and crack path tracking, the mechanisms responsible for the enhanced fatigue crack resistance in CHT Ti-6Al-4V-1Mo dual-phase alloy were discussed. In addition, the effects of near-spherical α-laths, discontinuous α grain boundary, and β_t matrix on fatigue crack deflection and branching were analyzed. This research provides insights into the microstructure design of laser-deposited titanium alloys and offers guidance for the development of aerospace materials with high damage tolerance.

2 Experiment

Pre-alloyed Ti-6Al-4V-1Mo powder with the particle size of 60.68±14.8 μm and chemical composition of 6.23Al-4.16V-0.996Mo-0.093O-balanced Ti (wt%) was used as the raw material. Before use, the powders were dried in a vacuum oven at 400 K for 12 h and sieved (sifter of 120 μm) to eliminate agglomerated particles. The substrate was a forged Ti-6Al-4V alloy with dimensions of 130 mm×130 mm×30 mm. After grinding with 280#–600# sandpaper, the substrate was sequentially cleaned by ultrasonic treatment in anhydrous ethanol and acetone to remove surface oxides and contaminants.

Fig. 1 shows the schematic diagrams of DED system, compact tension specimen, and CHT. DED experiments were conducted using a YSL-3000 fiber laser system, equipped with a 2 kW IPG fiber laser, a four-axis CNC platform, and a coaxial powder-feeding nozzle. The key process parameters are summarized in Table 1. The deposition process was

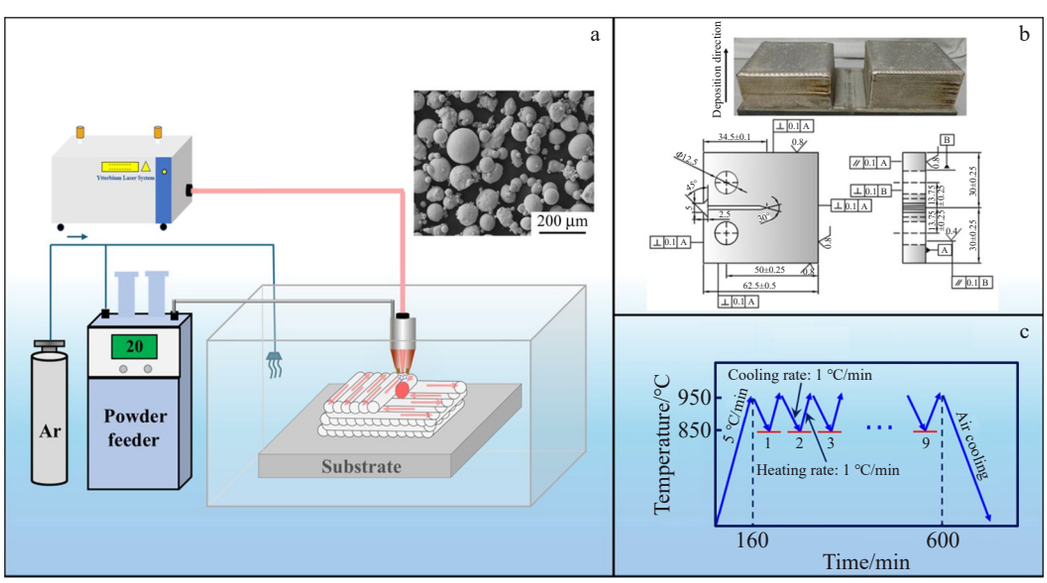

Fig.1 Schematic diagrams of DED system (a), compact tension specimen (b), and CHT process (c)

Table 1 DED process parameters for Ti-6Al-4V-1Mo alloy

Laser power/W	Scanning speed/mm·s^{-1}	Laser spot diameter/mm	Powder feeding rate/g·min^{-1}	Carrier gas flow rate/L·min^{-1}	*Z*-axis increment/mm
1800	4.2	3	5.5	10	0.5

conducted in an argon-protected chamber, maintaining oxygen levels below 0.01vol% and using the bidirectional scanning strategy. Specimens of 70 mm×70 mm×20 mm were fabricated layer by layer on the Ti-6Al-4V-1Mo alloy substrate.

CHT of the as-deposited specimens was performed using the KXL-1200X-J box furnace. Before designing the heat treatment schedule, the phase transformation temperature range of the Ti-6Al-4V-1Mo alloy was determined as 980 – 985 °C using JMat-Pro software in conjunction with metallographic analysis[24], as presented in Fig. 2. A maximum cyclic temperature of 950 °C, which is slightly below the phase transformation temperature, was selected for the heat treatment. Before heat treatment, the specimen surfaces were coated with a SiO_2 anti-oxidation layer. The specimens were subsequently subjected to cyclic thermal processing: heating to 950 °C (heating rate of 5 °C·min^{-1} and holding for 160 min) and then slow cooling to 850 °C (cooling rate of 1 °C·min^{-1} and holding for 100 min). This heating-cooling cycle was repeated 9 times. After the final cycle, the specimens were air-cooled to room temperature as the completion of CHT. The detailed heat treatment process is shown in Fig.1c.

Fatigue crack growth tests were conducted in accordance with GB/T 6398-2017. The specimens were machined into compact tension specimens, as shown in Fig. 1b, with a width (W) of 50 mm, a thickness (B) of 12.5 mm, and an initial crack length (a_0) of 12.5 mm. Testing was conducted using the MTS810 servo-hydraulic testing machine under the following conditions: stress ratio R=0.1, maximum load P_{max}=6.5 kN, and loading frequency f=15 Hz. The loading direction was perpendicular to the deposition direction.

To observe the microstructure, the as-deposited and cyclic heat-treated specimens were cut perpendicularly to the deposition direction. Microstructure observations were conducted using a Keyence VH-250L optical microscope (OM) and a Hitachi-S4800 scanning electron microscope (SEM). To analyze the fatigue crack growth path, OM specimens were taken near the fracture surface along the direction of the primary crack, and the non-fatigued specimens were prepared by the same process.

3 Results and Discussion

3.1 Microstructure

Fig. 3 shows the primary columnar β grains in the as-deposited and CHT Ti-6Al-4V-1Mo alloy specimens. As shown in Fig. 3a, the as-deposited specimen exhibits good surface quality with no visible macroscopic defects, such as pores or cracks. However, the non-equilibrium rapid solidification and complex thermal cycling inherent to DED result in the distinct epitaxial growth of the primary β grains[30]. Columnar β grains exhibit an average width of approximately 890.2 μm. Since the heat treatment temperature of 950 °C is below the β transition temperature, it is difficult to significantly alter the size and morphology of β grains through heat treatment alone in the absence of external plastic deformation[25]. As a result, the morphology of the columnar β grains remains essentially unchanged after CHT: the width reduces slightly to approximately 869.2 μm, as shown in Fig. 3c. Besides, significant changes can be observed in the morphology of α_{GB} after CHT, as shown in Fig. 3c – 3d. Unlike the continuous α_{GB} along β grain boundaries in the as-deposited specimen, the α_{GB} becomes discontinuous and significantly widened from approximately 2 μm to approximately 7 μm in size. This morphology change may result in different fatigue behavior between the as-deposited and CHT specimens. This transformation is attributed to the multi-step heat treatment

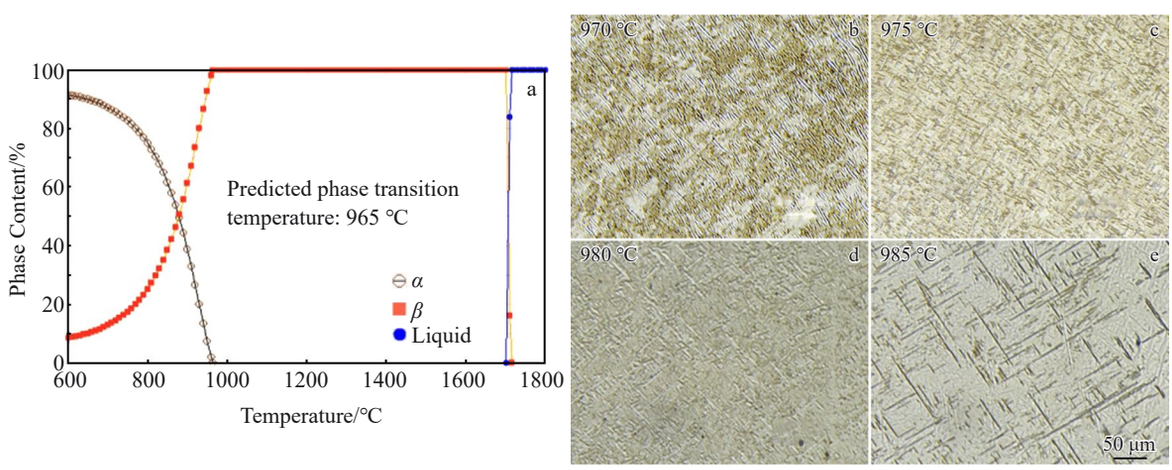

Fig.2 Prediction of β phase transition temperature of DED-prepared Ti-6Al-4V-1Mo alloy (a); microstructures of Ti-6Al-4V-1Mo alloy at 970 °C (b), 975 °C (c), 980 °C (d), and 985 °C (e)

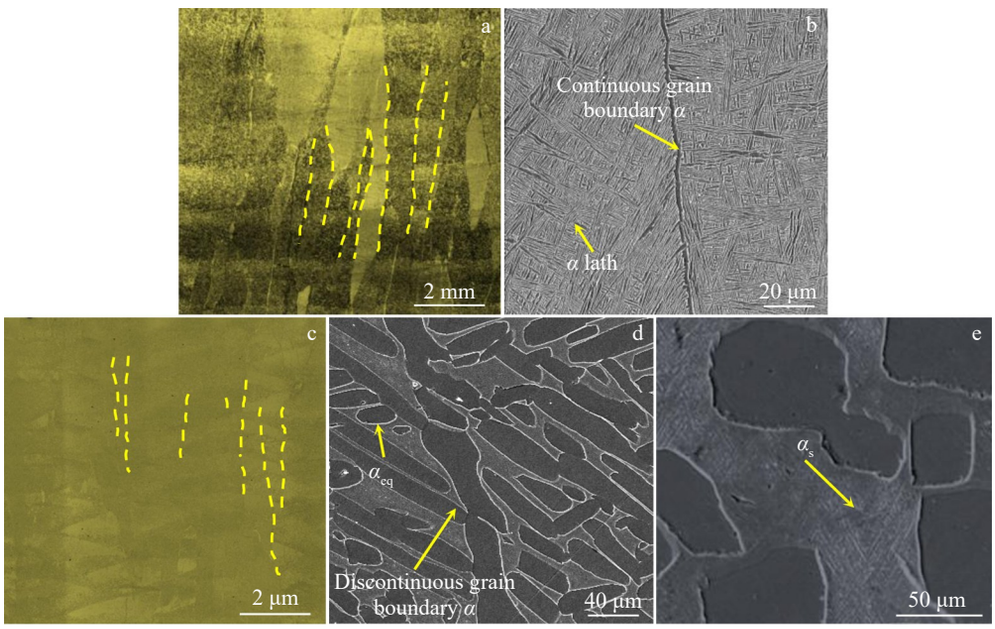

Fig.3 Morphologies of primary columnar β grains in as-deposited (a–b) and CHT (c–e) DED-prepared Ti-6Al-4V-1Mo alloys

conducted near the β transition temperature[26]. It is reported that the differences in crystallographic orientation and geometry between adjacent columnar β grains can cause incompatible plastic deformation, leading to stress concentration at continuous α_{GB}, which serves as a potential site for failure[27]. In contrast, discontinuous coarse α_{GB} can accommodate the deformation more effectively and interact with the surrounding microstructure. Compared to the continuous elongated α_{GB}, this configuration significantly delays crack propagation across grain boundaries, thereby enhancing fatigue crack resistance[28–29].

As shown in Fig.3b and 3d, the addition of Mo results in a uniform basket-weave α-lath structure in the as-deposited specimen. Compared to the conventional DED-prepared Ti-6Al-4V alloy, the Ti-6Al-4V-1Mo alloy has a finer and more homogeneous intragranular microstructure. The α-laths have an average width of approximately 0.8 μm and an average length of approximately 12.3 μm, yielding an average aspect ratio of 16.0. The α phase accounts for approximately 81vol% of the microstructure. CHT induces significant microstructure changes in the alloy specimens, as shown in Fig.3d–3e. The α-laths increase to approximately 8.0 μm in width and to approximately 21.9 μm in length. During the multi-step heat cycles, some intragranular α-laths are gradually spheroidized into near-spherical equiaxed α (α_{eq}). Different from the traditional processing methods that rely on deformation to introduce internal stress, AM leads to stress by the local thermal deformation caused by uneven temperature, which in turn generates residual stress as a driving force. Although there is no front-end thermal processing process, the spheroidization of the sub-grain boundary separation slab is essentially the same. At the same time, the solid-state phase transition caused by cyclic heating and cooling below β transition temperature during CHT also has a stress relaxation effect, thereby improving the fatigue performance of the material[31]. The spheroidization of α-laths follows a mechanism similar to the subgrain boundary separation mechanism. The substructures formed during DED are reactivated during CHT, resulting in the formation of subgrain boundaries within the primary α-laths. Ultimately, atomic diffusion causes the laths to separate and spheroidize[32–33]. After CHT, the primary α phase accounts for approximately 30.61vol% with an average aspect ratio of about 2.7. The spheroidized primary α phase, characterized by a larger width and a lower aspect ratio, exhibits enhanced deformation compatibility. Compared with the elongated α-laths, the spheroidized primary α phase can release the stress concentration more effectively, thereby improving the mechanical performance of the alloy[34–35].

Meanwhile, the fine secondary α (α_s) precipitates form within the retained β matrix, resulting in a distinct β-transformed microstructure, as shown in Fig.4. The α_s phase within the β matrix accounts for approximately 54.34vol% with an average width of 0.21 μm. Compared with the β phase in as-deposited specimen, the β-transformed microstructure generally demonstrates higher strength and enhanced resistance against the fatigue crack growth. In addition, the

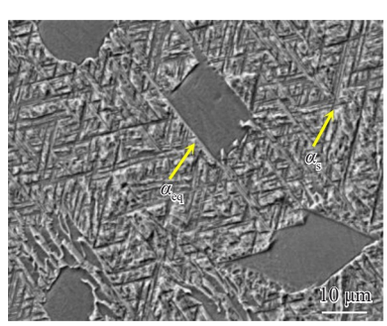

Fig.4 Intragranular microstructure of CHT Ti-6Al-4V-1Mo alloy

precipitation of fine needle-like α_s may alter the fatigue crack growth path, thereby lowering FCGR.

Fig. 5 shows the electron backscatter diffraction (EBSD) analysis of the Ti-6Al-4V-1Mo alloy after CHT. The inverse pole figure in Fig. 5b is acquired along the building direction and indicates that the coarse α_{GB} is fragmented by the heat treatment. Within the grains, the fragmentation of primary α-laths leads to the formation of near-equiaxed coarse α phases. Consequently, the intragranular structure is composed of multiple micro-textured regions with distinct orientations. The regions containing coarse and short α -laths with different orientations can deflect fatigue cracks to varying degrees during intragranular propagation, and the deflection degree depends on lath orientation and micro-texture boundaries. This deflection behavior is beneficial to the slow fatigue crack propagation.

3.2 FCGR

Fig. 6 presents FCGR curves of DED-prepared Ti-6Al-4V-1Mo alloys before (as-deposited) and after CHT. The Paris equation is widely used in engineering to evaluate an alloy's resistance against crack propagation in the steady-state fatigue crack growth region, which characterizes the relationship between FCGR and the nominal stress intensity factor range (ΔK), as follows:

$$\frac{\mathrm{d}a}{\mathrm{d}N} = C(\Delta K)^n \tag{1}$$

where a is crack length; N is the number of fatigue cycles; C and n are material-related constants. The constant C reflects inherent material properties and corresponds to the Y-axis intercept, whereas n represents the sensitivity of the crack growth rate to the changes in ΔK, corresponding to the slope of the linear region. A higher C value suggests that the material is more sensitive to the variations in ΔK.

Thus, FCGR expressions for the DED-prepared Ti-6Al-4V-1Mo alloys before and after CHT can be derived, as expressed by Eq.(2–3), respectively:

$$\frac{\mathrm{d}a}{\mathrm{d}N} = 1.8651 \times 10^{-8}(\Delta K)^{3.2271} \tag{2}$$

$$\frac{\mathrm{d}a}{\mathrm{d}N} = 1.4112 \times 10^{-8}(\Delta K)^{3.1125} \tag{3}$$

Both expressions show good fitting results, and the correlation coefficients are more than 0.99. As indicated by the fitted equations, the C and n values of CHT specimens are significantly smaller than those of the as-deposited ones, suggesting enhanced resistance against fatigue crack propagation. According to Fig. 6, da/dN and ΔK exhibit a nearly linear relationship, indicating that under a maximum applied load of 6.5 kN, the crack growth is in a stable propagation region. Compared with the as-deposited state, the da/dN-ΔK curves of CHT specimens show a distinct downward shift, reflecting a slower FCGR at the same ΔK. For the as-deposited specimens, the initial ΔK and da/dN are 14.3 MPa·m$^{1/2}$ and 1.17×10^{-4} mm/cycle, respectively. After CHT, the ΔK and da/dN decrease to 11.79 MPa·m$^{1/2}$ and 3.05×10^{-5} mm/cycle, respectively. At lower ΔK levels, CHT facilitates the residual stress release and promotes the formation of dual-phase microstructure, which in turn reduces local stress intensities at the crack tip, lowering the likelihood of crack propagation and initiation. Moreover, when the ΔK value ranges between 10–50 MPa·m$^{1/2}$, the da/dN values for CHT specimens range from 10^{-5} mm/cycle to 10^{-2} mm/cycle. Compared with that at the as-deposited state, the broader variation in ΔK further supports the enhancement in fatigue crack growth resistance of the alloy after CHT.

As shown in the fatigue crack growth paths in Fig.6, the as-deposited specimens exhibit a relatively straight crack trajectory from the notch tip of the compact tension specimen to the final fracture zone, where the path becomes markedly tortuous. FCGR under this condition is relatively fast. In contrast, CHT specimens exhibit a more tortuous crack path with greater deviation from the specimen centerline. This phenomenon suggests that the crack growth process in CHT specimens faces increased resistance, resulting in a significantly reduced FCGR, compared with that under the as-deposited condition.

3.3 Fracture morphology

To further explain the potential mechanism of crack propagation, macro- and micro-fracture morphologies of the compact tension specimens were analyzed. Fig. 7a and Fig. 8a present the appearances of the fracture surfaces of as-deposited and CHT specimens, respectively. The fatigue fracture surfaces clearly exhibit three distinct regions with the primary crack propagated from right to left side. In the near-threshold region, FCGR is slow, and the fracture surface appears relatively smooth. In the stable propagation region, the fracture surface changes from smooth to rough, indicating

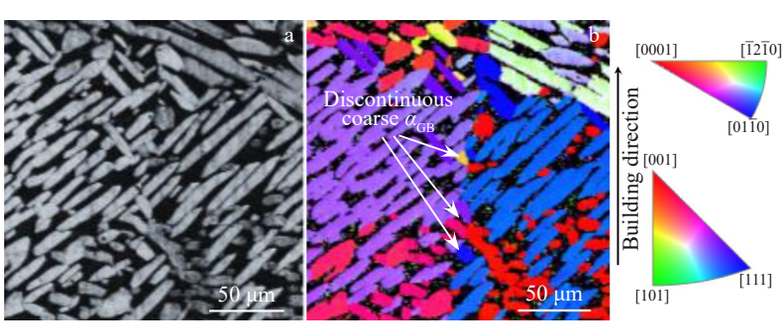

Fig.5 EBSD analysis of Ti-6Al-4V-1Mo alloy after CHT: (a) SEM image; (b) corresponding inverse pole figure along building direction

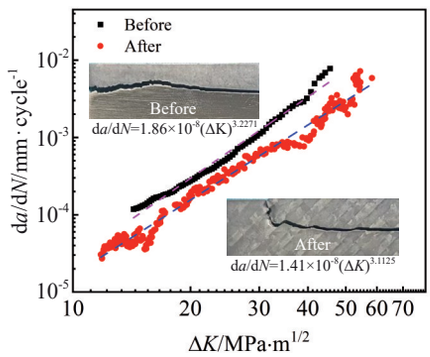

Fig.6 FCGR curves and appearances of crack propagation paths of DED-prepared Ti-6Al-4V-1Mo alloys before and after CHT

an increase in FCGR. In the final fracture region, FCGR is the fastest, and the fracture process is dominated by the applied external load and becomes less dependent on the microstructure. In addition, the fracture appearance shows pronounced tear-ridge features.

Fig. 7 shows the fracture morphologies of fatigue crack propagation at room temperature for the as-deposited DED-prepared Ti-6Al-4V-1Mo alloy. Fig. 7b–7d depict the fracture features in the near-threshold, steady-state growth, and final fracture regions, respectively. In Fig. 7b, the fracture surface in the near-threshold region reveals clear fatigue striations and numerous fine secondary cracks. The closely spaced fatigue striations suggest that the crack advances only a short distance per loading cycle, resulting in the slow FCGR at this stage. In the steady-state growth region, FCGR is increased with the increase in ΔK. The fatigue striations become coarser and are more widely spaced, compared with those in the near-threshold region. Additionally, both the number and size of secondary cracks increase, as illustrated in Fig. 7c. In the final fracture region (Fig. 7d), densely distributed fine dimples can be observed, surrounded by white tear ridges. This is the characteristic of ductile tensile fracture, indicating good plasticity of the specimen. Notably, fatigue striations are absent at this stage.

Fig. 8 shows fracture morphologies of CHT specimen during fatigue crack propagation. Fig. 8b – 8d illustrate the fracture features in the near-threshold, steady-state growth, and final fracture regions, respectively. Compared with the as-deposited specimen, CHT specimen demonstrates a slower FCGR. As shown in Fig. 8a, the fracture surface of CHT specimen reveals distinct columnar grain features and greater surface roughness, compared with that of the as-deposited specimen. In the near-threshold region (Fig. 8b), frictional marks are observed, possibly indicating crack closure effects. Additionally, very fine fatigue striations and secondary cracks are visible. In the crack propagation region (Fig. 8c), typical fatigue striations are observed with spacing larger than those in the as-deposited specimen. The presence of more secondary cracks in this region indicates a diminished crack driving force, thereby contributing to the reduced FCGR[33]. In the final fracture region (Fig. 8d), typical dimple features are observed, and the dimples and tear ridges are larger and deeper than those in the as-deposited specimen. These phenomena suggest that CHT improves the specimen toughness, thereby enhancing the resistance against fatigue crack propagation.

3.4 Crack propagation path

In the stable crack growth region, the fatigue crack interacts with the alloy microstructure during propagation, as illustrated in Fig. 9–Fig. 10. The primary cracks are propagated from left to right side.

When the stress ratio (R), frequency (f), and other experiment parameters are set as constant, the fatigue crack propagation path is primarily governed by the material

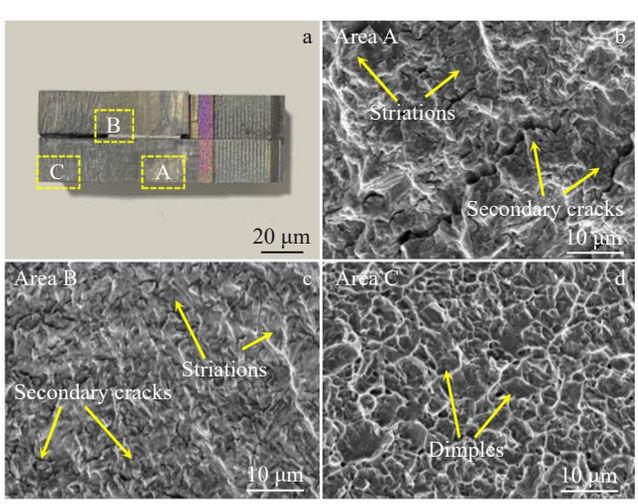

Fig.7 Fracture morphologies of as-deposited DED-prepared Ti-6Al-4V-1Mo alloy: (a) appearance; (b) microstructure near-threshold region; (c) microstructure in steady-state growth region; (d) microstructure in final fracture region

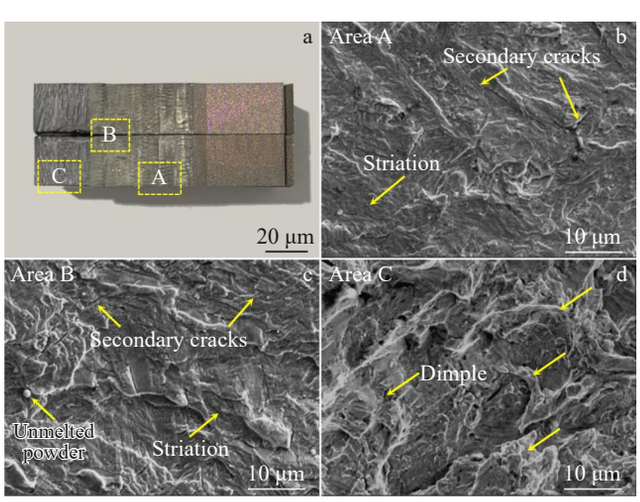

Fig.8 Fracture morphologies of CHT DED-prepared Ti-6Al-4V-1Mo alloy: (a) appearance; (b) microstructure near-threshold region; (c) microstructure in steady-state growth region; (d) microstructure in final fracture region

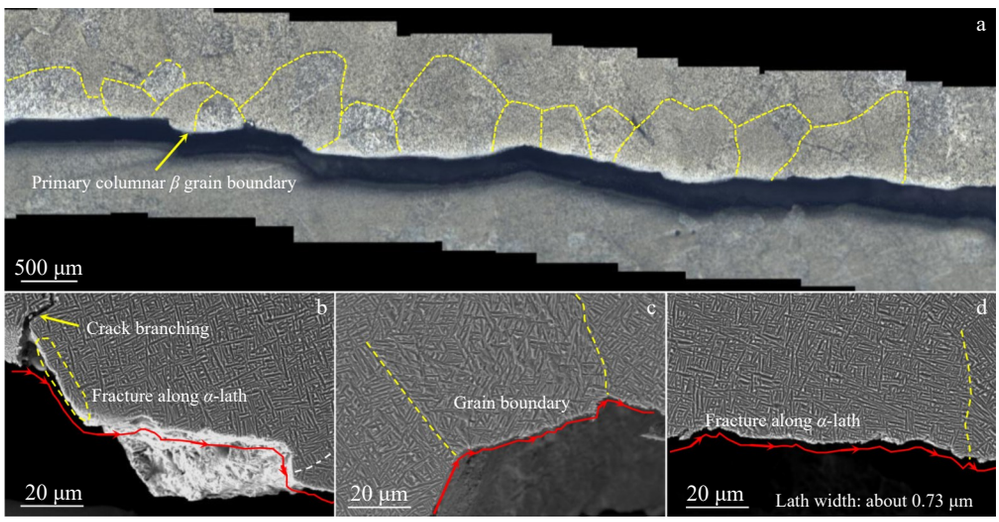

Fig.9 Fatigue crack propagation behavior of as-deposited DED-prepared Ti-6Al-4V-1Mo alloy: (a) macrostructure; (b–d) interactions between crack and microstructure

microstructure. With the Mo addition, the intragranular microstructure of the Ti-6Al-4V alloy exhibits a fine basket-weave structure. Notably, when the crack tip encounters a grain boundary, it deflects, and the subsequent propagation path within the grain depends on the scale and morphology of the intragranular laths. Further observations of the as-deposited specimens reveal that the deflection of the crack tip often leads to the formation of secondary cracks, whose propagation directions differ from those of the primary cracks. This mechanism effectively reduces stress concentration and delays the crack propagation[37], as shown in Fig.9b. When the angle between the intragranular α-laths and the crack propagation direction is small, crack resistance is reduced, and the crack tends to propagate along the lath boundaries. However, as the angle between the lath direction and the crack path increases, cracks are more likely to traverse the elongated α-laths, which have an average width of approximately 0.8 μm in the as-deposited specimen. Additionally, the complexity of the basket-weave structure and the lath distribution leads to alternating propagation modes, resulting in a zigzag crack path, as shown in Fig. 9d. However, due to the overall finer lath structure, the crack path remains relatively flat.

In addition to the intragranular microstructure, the influence of large columnar grains with varying orientations on crack propagation must also be considered. It is reported that the orientation of primary columnar β grains can negatively influence FCGR, and the angle between the grain boundary and the crack propagation direction plays a critical role in determining the reduction degree. As shown in Fig. 9a and 9c, when the crack reaches the interface between columnar β grains, its propagation path tends to become perpendicular to the grain orientation. The crack traverses the grain boundaries, and each crossing results in a deflection of the propagation path, as indicated by the yellow dashed lines in Fig. 9. This deflection is more pronounced than that caused by the intragranular structure, because the grain boundaries impede crack growth by altering the local stress field, resulting in uneven stress distribution among grains and enhanced crack path deflection. This behavior is consistent with the results in Ref.[38] during fatigue crack growth testing of electron beam-melted Ti-6Al-4V alloy. Therefore, for the as-deposited Ti-6Al-4V-1Mo specimens, the tortuosity of the crack propagation path is primarily influenced by the obstruction posed by differently oriented grains, whereas the uniformly distributed fine intragranular laths provide comparatively lower resistance against fatigue crack growth, leading to a relatively straighter crack path.

Microstructure analysis of Ti-6Al-4V-1Mo alloy after CHT reveals that the intragranular laths become coarser, and a dual-phase microstructure consisting of near-spherical α and β-transformed matrix phases is formed. This microstructure change markedly enhances the resistance against fatigue crack propagation. In conjunction with the crack path analysis of the as-deposited specimens, it can be concluded that the coarser near-spherical α and strengthened matrix contribute substantially to the enhanced fatigue crack growth resistance. At this stage, the lath width increases to approximately 8.0 μm, which is nearly ten times larger than that of the as-deposited specimen. As shown in Fig. 10b, when the angle between the near-spherical α phase and the crack tip is small, the crack is propagated smoothly along the phase boundary. However, when the crack traverses the grain boundaries, the coarse near-spherical α phase induces greater deflection of the crack path. The fatigue crack path exhibits more significant deflection, curving downward to the right side and forming a distinctive Z-shaped trajectory[39]. Additionally, secondary cracks are initiated before the crack tip, which can reduce the stress concentration and facilitate the further deflection of the main crack path[40]. As the crack continues to propagate, the orientation of the spherical α phase forms a certain angle with the crack path, resulting in a more pronounced zigzag trajectory, compared with that in the as-deposited specimen.

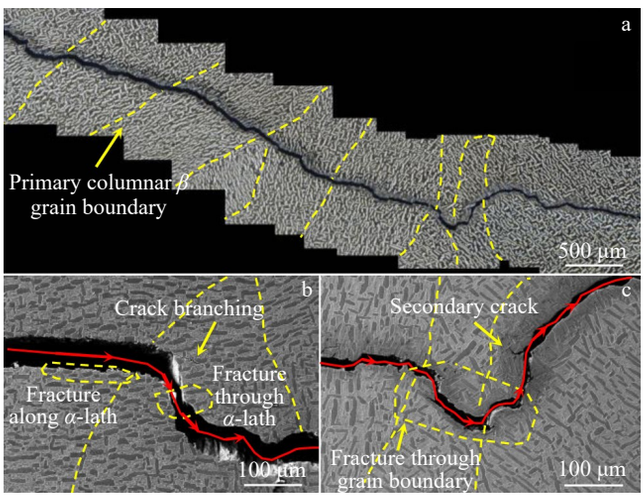

Fig.10 Fatigue crack growth behavior of CHT DED-prepared Ti-6Al-4V-1Mo alloy: (a) macrostructure; (b–c) interactions between crack and microstructure

Fig. 10c illustrates the continuous local crack deflection influenced by the microstructure, which arises from the combined effects of grain boundary traversing and interaction with intragranular laths. When the crack crosses a grain boundary, it deflects downward to the right side; within the grain, it follows the laths parallel to the crack tip. Upon reaching the next grain, the crack deflects upward again, and the lath orientation forms a new angle with the crack front. The crack advances in a zigzag pattern until it traverses the coarse-grained material. This continuous large-angle deflection coupled with the obstructive effect caused by discontinuous coarse α_{GB} significantly reduces FCGR at this stage[29].

Unlike the typical AM microstructure in the as-deposited specimens, which is characterized by primary columnar β grains and uniformly distributed intragranular basket-weave structures, CHT specimens exhibit a dual-phase microstructure consisting of near-spherical α and β-transformed matrix phases. Owing to the mechanical mismatch between these two phases, crack branching occurs when the main crack reaches the phase boundary. As shown in Fig. 11a, the secondary cracks have an angel of approximately 90° to the main cracks. These secondary cracks with different directions from the main cracks effectively reduce the stress concentration, dissipate the energy at crack tip, and consequently retard the crack propagation[41]. Additionally, continuous cyclic loading may initiate small cracks along phase boundaries, as shown in Fig.11b, which further contribute to the deceleration of fatigue crack propagation. Both types of cracks are propagated under cyclic loading, and their growth consumes the available crack-driving force, further reducing the propagation rate of the main fatigue crack. As illustrated in Fig. 11c, during intragranular propagation, the crack tip undergoes convergence at specific sites, forming a crack-bridging phenomenon, which contributes to the crack arrest. Secondary cracks, once deflected by the surrounding microstructure, may reconnect with the main crack path, further hindering the crack growth. In summary, compared with the fine basket-weave structure of elongated α phase in the as-deposited specimen, the dual-phase microstructure of near-spherical α and β-transformed matrix phases in CHT specimens offers superior resistance against fatigue crack propagation. The enhanced deflection and crack-growth resistance significantly reduce the final FCGR[42–43].

Fig.12 presents the schematic diagrams of the fatigue crack propagation mechanism. In the as-deposited DED-prepared Ti-6Al-4V-1Mo alloy, the fatigue crack propagation behavior is predominantly governed by the microstructure features. The intragranular microstructure in the as-deposited specimen contains a fine basket-weave structure. However, the fine scale of the laths restricts the overall tortuosity of the crack path, and the deflection and obstruction caused by these features are minimal, resulting in relatively low fatigue crack growth resistance. At this stage, resistance against crack propagation primarily arises from deflections at the grain boundaries of the primary columnar β grains and the random orientations of the intragranular α phase. After CHT at 950 °C for 9 cycles, the microstructure is transformed into a dual-phase structure composed of near-spherical α and β-transformed matrix, and the α-laths are coarsened to about 8.0 μm in size, exhibiting more random orientations. This coarser microstructure substantially enhances the tortuosity of the fatigue crack propagation path. Additionally, the formation of secondary cracks and microcracks along phase boundaries dissipates energy and reduces the driving force at the crack tip, while the synergistic interaction between the matrix and

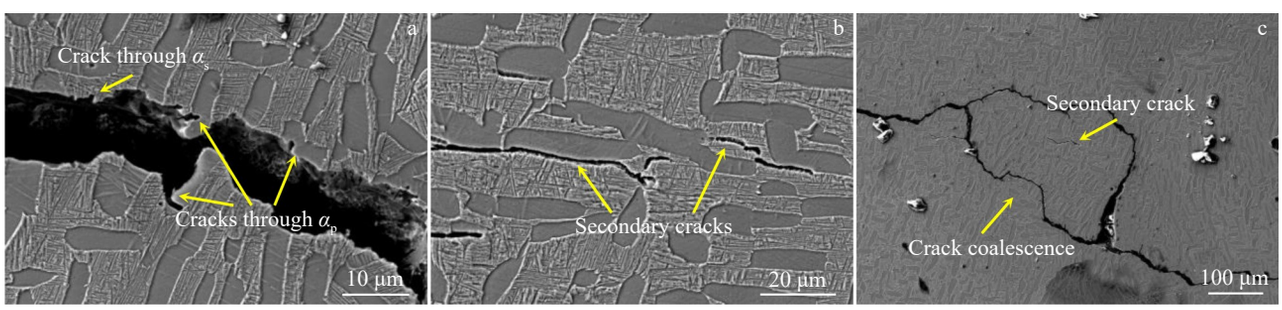

Fig.11 Interactions between crack propagation and microstructures in CHT DED-prepared Ti-6Al-4V-1Mo alloy: (a) cracks crossing α phases; (b) secondary cracks along phase boundary; (c) crack bridging phenomenon

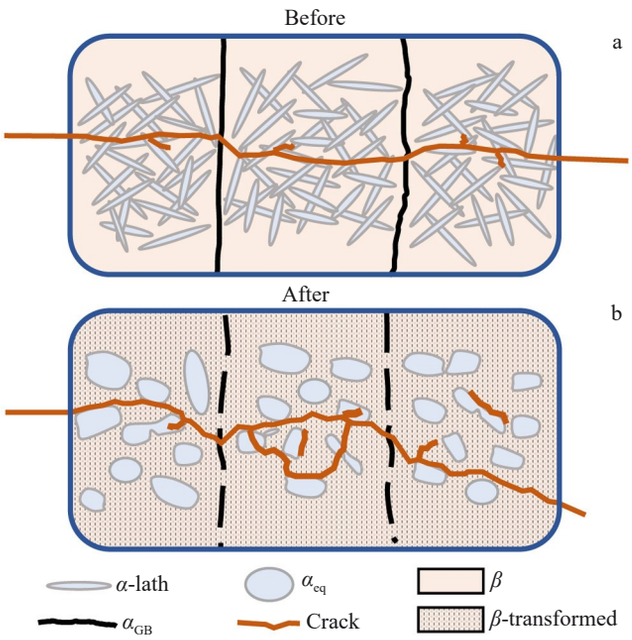

Fig.12 Schematic diagrams of fatigue crack propagation of DED-prepared Ti-6Al-4V-1Mo alloy before (a) and after (b) CHT

coarsened α-laths further extends the propagation path. The observed crack-bridging phenomenon redistributes the local stress field and lowers the stress intensity factor at the crack tip. In this research, CHT specimens exhibit multiple mechanisms of fatigue crack growth resistance, including increased path tortuosity, interfacial energy dissipation, and synergistic hindrance effects, which collectively result in a marked improvement in crack growth resistance. These findings offer a theoretical foundation for optimizing the fatigue design strategies in AM titanium alloys.

4 Conclusions

1) The as-deposited DED-prepared Ti-6Al-4V-1Mo alloy features epitaxially grown primary β columnar grains, continuous α phases along grain boundaries, and a fine intragranular basket-weave structure. After CHT, the β grain morphology is basically unchanged, but the grain boundary α phase becomes discontinuous, and the α -laths coarsen, forming a dual-phase microstructure of near-spherical α and β-transformed matrix phases.

2) FCGR in the stable propagation region follows the Paris law: $da/dN=1.8651\times10^{-8}(\Delta K)^{3.2271}$ for the as-deposited specimen, and $da/dN=1.4112\times10^{-8}(\Delta K)^{3.1125}$ for CHT specimen. Compared with the as-deposited specimen, CHT specimen exhibits a more tortuous crack propagation path with greater deviation from the centerline, enhancing the resistance against fatigue crack growth.

3) Crack deflection occurs when the crack crosses grain boundaries due to boundary resistance, and this effect becomes more pronounced when the α_{GB} is discontinuous and coarser. The influence of the intragranular structure depends on both the angle between the crack propagation direction and the α-lath orientation and the scale of the laths. Larger angle and coarser laths result in greater resistance against the fatigue crack propagation.

References

1 Gu D D, Shi X Y, Poprawe R *et al*. *Science*[J], 2021 372(6545): 1487
2 Herzog D, Seyda V, Wycisk E *et al*. *Acta Materialia*[J], 2016, 117: 371
3 Simonelli M, Tse Y Y, Tuck C. *Metallurgical and Materials Transactions A*[J], 2014, 45: 2863
4 Yang J J, Yu H C, Yin J *et al*. *Materials & Design*[J], 2016, 108: 308
5 Azarniya A, Colera X G, Mirzaali M J *et al*. *Journal of Alloys and Compounds*[J], 2019, 804: 163
6 Liu S, Shin Y C. *Materials & Design*[J], 2019, 164: 107552
7 Kok Y, Tan X P, Wang P *et al*. *Materials & Design*[J], 2018, 139: 565
8 Nguyen H D, Pramanik A, Basak A K *et al*. *Journal of Materials Research and Technology*[J], 2022, 18: 4641
9 Han J, Zhang G Y, Chen X Y *et al*. *Journal of Materials Processing Technology*[J], 2022, 310: 117759
10 Wang X, Zhang L J, Ning J *et al*. *Additive Manufacturing*[J], 2021, 48: 102442
11 Narayana P L, Lee S W, Choi S W *et al*. *Journal of Alloys and Compounds*[J], 2019, 811: 152021
12 Vrancken B, Thijs L, Kruth J P *et al*. *Acta Materialia*[J], 2014, 68: 150
13 Li G C, Li J, Tian X J *et al*. *Materials Science and Engineering A*[J], 2017, 684: 233
14 Ye Z M, Yu Z R, Gao P P *et al*. *Additive Manufacturing*[J], 2024, 86: 104226
15 Xia C, Zhao K X, Zhou X *et al*. *Acta Metallurgica Sinica* (*English Letters*)[J], 2024, 37(1): 119
16 Guo P, Zhao Y Q, Zeng W *et al*. *Journal of Materials Engineering and Performance*[J], 2015, 24(5): 1865
17 Kim S, Oh H J, Kim J G *et al*. *Metals and Materials International*[J], 2021, 28(1): 205
18 Liu J W, Zhang K, Liu J *et al*. *International Journal of Fatigue*[J], 2023, 176: 107839
19 Liu Z, Dash S S, Zhang J *et al*. *International Journal of Plasticity*[J], 2024, 172: 103819
20 Sahil D, Milan B, Daniel F *et al*. *Acta Materialia*[J], 2025, 297: 121372
21 Yue L S, Zhou Q J, Pan Y *et al*. *International Journal of Fatigue*[J], 2024, 188: 108518
22 Sabban R, Bahl S, Chatterjee K *et al*. *Acta Materialia*[J], 2019, 162: 239
23 McKenna T, Tomonto C, Duggan G *et al*. *Materials & Design*[J], 2023, 227: 111700
24 Zhang F Y, Wang K, Li Y *et al*. *Journal of Materials Processing*

Technology[J], 2022, 299: 117321
25 Brandl E, Greitemeier D. *Materials Letters*[J], 2012, 81: 84
26 Sun Y N, Pan S W, Hao P F *et al*. *Materials Today Communications*[J], 2025, 44: 112106
27 Carroll B E, Palmer T A, Beese A M. *Acta Materialia*[J], 2015, 87: 309
28 Xie Y, Gong M C, Zhang R Z *et al*. *Journal of Alloys and Compounds*[J], 2021, 869: 159287
29 Li Z, Tian X J, Tang H B *et al*. *Transactions of Nonferrous Metals Society of China*[J], 2013, 23(9): 2591
30 Zhang Fengying, Yang Sen, Huang Kaihu *et al*. *Rare Metal Materials and Engineering*[J], 2022, 51(6): 2105 (in Chinese)
31 Chen S G, Zhang Y D, Wu Q *et al*. *Materials Science and Engineering A*[J], 2021, 819: 141299
32 Weiss I, Froes F H, Eylon D *et al*. *Metallurgical Transactions A*[J], 1986, 17(11): 1935
33 Stefansson N, Semiatin S L. *Metallurgical and Materials Transactions A*[J], 2003, 34(3): 691
34 Liu C M, Tian X J, Wang H M *et al*. *Materials Science and Engineering A*[J], 2014, 609: 177
35 Zhao Z, Chen J, Tan H *et al*. *Scripta Materialia*[J], 2018, 146: 187
36 Gao Wenzhu, Wu Huan, Zhao Yongqing. *Titanium Industry Progress*[J], 2007, 24(6): 33 (in Chinese)
37 Meng X, Yang S L, Huang Y B *et al*. *Materials Chemistry and Physics*[J], 2020, 257: 123734
38 Galarraga H, Warren R J, Lados D A *et al*. *Engineering Fracture Mechanics*[J], 2017, 176: 263
39 Wang K, Bao R, Jiang B *et al*. *International Journal of Fatigue*[J], 2018, 116: 535
40 Xu Liang, Huang Shuangjun, Wang Lei *et al*. *Rare Metal Materials and Engineering*[J], 2017, 46(7): 1943 (in Chinese)
41 Li Hui, Zhao Yongqing, Qu Henglei *et al*. *Titanium Industry Progress*[J], 2005, 22(6): 10 (in Chinese)
42 Shi Puying, Chen Lin, Liu Xianghong *et al*. *Rare Metal Materials and Engineering*[J], 2024, 53(10): 2823 (in Chinese)
43 Guo Ping, Zhang Jingli, Qiang Fei *et al*. *Rare Metal Materials and Engineering*[J], 2022, 51(11): 4358 (in Chinese)

循环热处理对激光定向能量沉积Ti-6Al-4V-1Mo合金疲劳裂纹扩展速率的影响

薛立攀，张凤英，邓雨林，叶梓萌，赵可馨，余泽镕，武文璐，苏　伟，杨仁洁
(长安大学 材料科学与工程学院，陕西 西安 710064)

摘　要：对一种面向激光定向能量沉积的新型Ti-6Al-4V-1Mo钛合金循环热处理前后的疲劳裂纹扩展速率进行了研究，分析了循环热处理前后显微组织的变化及疲劳裂纹扩展试样的断口和扩展路径。结果显示：沉积态与循环热处理试样裂纹扩展速率在稳定扩展区的表达式分别为$\mathrm{d}a/\mathrm{d}N=1.8651\times10^{-8}(\Delta K)^{3.2271}$和$\mathrm{d}a/\mathrm{d}N=1.4112\times10^{-8}(\Delta K)^{3.1125}$。与沉积态相比，循环热处理后合金微观组织从均匀编织的网篮组织转变为由近球状α与β转化基体组成的双态组织，初生β晶界处的晶界α相连续性也在循环过程中被打断。循环热处理后初生α的粗化及非连续晶界α相是缓解应力集中、偏转疲劳裂纹的主要原因，由此导致疲劳裂纹扩展。此外，循环热处理试样中更易出现的裂纹分支、二次裂纹及裂纹桥接也是降低疲劳裂纹扩展的驱动力，是减缓裂纹扩展速率的重要原因。

关键词：Ti-6Al-4V-1Mo钛合金；循环热处理；疲劳裂纹扩展速率；激光定向能量沉积

作者简介：薛立攀，男，2001年生，硕士，长安大学材料科学与工程学院，陕西 西安 710064，E-mail：1647163062@qq.com